Eur. Phys. J. A **38**, 209–217 (2008)
DOI 10.1140/epja/i2008-10662-x

THE EUROPEAN PHYSICAL JOURNAL A

Regular Article – Experimental Physics

np $\longrightarrow \eta$d near threshold and the s-wave ηN amplitude

H. Garcilazo[1,a] and M.T. Peña[2]

[1] Escuela Superior de Física y Matemáticas, Instituto Politécnico Nacional, Edificio 9, 07738 México D.F., Mexico
[2] Instituto Superior Técnico, Centro de Física Teórica de Partículas, and Department of Physics, Av. Rovisco Pais, 1049-001 Lisboa, Portugal

Received: 26 June 2008 / Revised: 22 September 2008
Published online: 30 October 2008 – © Società Italiana di Fisica / Springer-Verlag 2008
Communicated by M. Anselmino

Abstract. We calculate the process $np \to \eta d$ near threshold using a separable potential model of the coupled $\eta N - \pi N - \pi\pi N$ subystems, and a relativistic three-body calculation for the ηd scattering amplitude. The $\pi\pi N$ channels are represented by an effective σN channel, and we compare the case where the σ and π masses are related by $m_\sigma = 2m_\pi$ and no width is considered, to another where the mass and width of the σ-meson are taken from $\pi\pi$ scattering data. The $np \to \eta d$ cross-section can be well described up to about 60 MeV by models where the real part of the ηN scattering length lies between $0.4 \leq \mathrm{Re}(a_{\eta N}) \leq 0.6$ fm which allows us to determine the s-wave ηN scattering amplitude for $-60 \leq E \leq 60$ MeV.

PACS. 21.30.Fe Forces in hadronic systems and effective interactions – 21.45.-v Few-body systems – 25.10.+s Nuclear reactions involving few-nucleon systems – 11.80.Jy Many-body scattering and Faddeev equation

1 Introduction

In a recent paper we have developed a model of the $np \to \eta d$ process within the framework of a relativistic three-body theory of the ηNN system [1]. That study proceeded within the program [2,3] of using the high-quality data [4] now available for reactions with ηN interactions in the final states to constrain the two-body dynamics of this meson-nucleon system. The two main conclusions of that work were that a) near threshold the shape of the $np \to \eta d$ cross-section is determined essentially by the three-body ηd final-state interaction as a consequence of Watson's theorem [5] and b) the $np \to \eta d$ data indicates that, among all the existing models [6–9] explaining the two-body ηN amplitude, the most appropriate one for the description of the more complex meson production reaction $np \to \eta d$ lies between the models with scattering lengths of 0.42 [6] and 0.72 fm [7]. This conclusion gives valuable information on the strength of the ηN interaction, since the two limiting models are characterized by a small value for the real part of the ηN scattering length. To furthermore explore the energy dependence of the ηN interaction, by carefully determining the values of the effective-range parameters indeed demanded by the data, the calculational scheme of ref. [1], although already including a relativistic treatment, still lacks important improvements.

In this context, here we firstly will take into account the unstable nature of the σ-meson by including its width using the replacement $m_\sigma \to m_\sigma - i\Gamma(\sqrt{s_\sigma})$ where the mass and width of the σ-meson are determined from the data for $\pi\pi$ scattering. This way the role of the $\pi\pi$ channel is more realistically considered. Secondly, we will generate additional two-body ηN-ηN scattering amplitudes, interpolating the amplitudes originated by the existing data analyses. This allowed us not only to investigate more precisely the effect of the ηN scattering length on the $np \to \eta d$ cross-section, but also the role of the other ηN effective-range parameters that determine the energy dependence. This progress sophisticated the capability of our calculation to describe the $np \to \eta d$ cross-section as a function of energy, and simultaneously improved our knowledge on the ηN interaction.

In the analysis of ref. [1] we considered seven models of the ηN scattering amplitude labeled 0–6 which are characterized by the predicted value of the ηN scattering length $a_{\eta N}$. Model 0 was based on a Jülich group data analysis [6] of πN scattering which has been meanwhile updated and improved in ref. [10], and such changes needed to be taken into account. In the present work we used this newer version which describes much more satisfactorily the inelasticity parameter in the S_{11} partial wave, the relevant one for η production. Besides, as a result of a more adequate treatment of the $\pi\pi N$ channel, this new version does not overestimate the $\pi N \to \eta N$ transition, as the previous version did. This correction modifies the role played by

[a] e-mail: humberto@esfm.ipn.mx

Table 1. Effective-range parameters of the seven models of the ηN amplitude.

Model	Ref.	$a_{\eta N}$(fm)	$r_{\eta N}$(fm)	$s_{\eta N}$(fm^3)
0	[10]	$0.407 + \mathrm{i}0.255$	$-3.442 + \mathrm{i}0.320$	$0.202 - \mathrm{i}0.124$
1	[7]	$0.717 + \mathrm{i}0.264$	$-1.594 - \mathrm{i}0.028$	$-0.014 - \mathrm{i}0.015$
2	[8]	$0.75 + \mathrm{i}0.27$	$-1.50 - \mathrm{i}0.24$	$-0.10 - \mathrm{i}0.01$
3	[9]	$0.83 + \mathrm{i}0.27$	$-1.34 - \mathrm{i}0.22$	$-0.12 - \mathrm{i}0.01$
4	[9]	$0.87 + \mathrm{i}0.27$	$-1.31 - \mathrm{i}0.28$	$-0.14 - \mathrm{i}0.03$
5	[9]	$1.05 + \mathrm{i}0.27$	$-1.19 - \mathrm{i}0.31$	$-0.18 - \mathrm{i}0.06$
6	[9]	$1.07 + \mathrm{i}0.26$	$-1.25 - \mathrm{i}0.25$	$-0.20 - \mathrm{i}0.05$

that transition as a building block of the mechanisms of the $np \to \eta d$ reaction. The ηN elastic scattering amplitude $f_{\eta N}$ is given by the effective-range formula

$$f_{\eta N}^{-1} = \frac{1}{a_{\eta N}} + \frac{1}{2} r_{\eta N} p^2 + s_{\eta N} p^4 - ip, \tag{1}$$

where p is the c.m. relative momentum and the parameters $a_{\eta N}$, $r_{\eta N}$, and $s_{\eta N}$ of the seven models 0–6 as well as the references to each model are given in table 1.

Section 2, below, presents the relativistic formalism of the $np \to \eta d$ reaction while sect. 3 outlines the new aspects introduced in the calculation. Finally, in sect. 4 we present the results.

2 Relativistic formalism

In the $np \to \eta d$ process the total isospin is equal to zero so that in the region very near the threshold the η and the d are in a state of relative orbital angular momentum $L = 0$ which implies that the initial np state must be in the $^1P_1$ state. Our formalism of the $np \to \eta d$ process consists of the production operator, the ηd final-state interaction, and the np initial-state interaction. We will describe separately each one of these aspects of the formalism.

2.1 The production mechanism

The basic mechanism of the $np \to \eta d$ reaction is the triangle diagram [11] where in the initial np state (formed by nucleons 2 and 3) nucleon 2 emits a meson m ($m = \eta, \pi, \sigma$) which interacts with nucleon 3 to produce the η by means of the amplitude $mN \to \eta N$ while nucleon 2 remains as spectator (now as nucleon N). The final nucleon in the $mN \to \eta N$ amplitude (nucleon M) then forms the deuteron with the spectator nucleon N.

We evaluate the triangle diagram by putting the spectator nucleon on its mass shell; thus, the four-dimensional integral reduces to the integration in the three-momentum $\vec{k}_N$ of that nucleon as

$$A_{M_d}^{\mu_2\mu_3} = \frac{1}{(2\pi)^3} \sum_{\nu} \int \mathrm{d}\vec{k}_N \frac{M}{E_N} \bar{v}_N^{\nu} V_{dNN}^{M_d} \frac{\not{k}_M + M}{k_M^2 - M^2} t_{mN\to\eta N} u_3^{\mu_3} \times \frac{1}{k_m^2 - m_m^2} \bar{u}_N^{\nu} V_{mNN} u_2^{\mu_2}\,, \tag{2}$$

where $V_{dNN}^{M_d}$ and V_{mNN} are, respectively, the deuteron-nucleon-nucleon and the m meson-nucleon-nucleon vertices. The spinors $u_2^{\mu_2}$, $u_3^{\mu_3}$, $\bar{u}_N^{\nu}$, correspond, respectively, to the two initial and the spectator nucleon spinors, and $\bar{v}_N^{\nu}$ is the charge-conjugated spinor [11].

Since the final η is restricted to the energy region $E < 60\,\mathrm{MeV}$, the effects of relativity are not so crucial for the nucleon M. Therefore, we will write the propagator of that nucleon in terms of positive and negative energy spinors and keep only the positive energy part:

$$\begin{aligned}\frac{\not{k}_M + M}{k_M^2 - M^2} &= \frac{M}{E_M} \sum_{\mu} \frac{u_M^{\mu}(\vec{k}_M)\bar{u}_M^{\mu}(\vec{k}_M)}{k_{0M} - E_M} \\ &\quad + \frac{M}{E_M} \sum_{\mu} \frac{v_M^{\mu}(-\vec{k}_M)\bar{v}_M^{\mu}(-\vec{k}_M)}{k_{0M} + E_M} \\ &\to \frac{M}{E_M} \sum_{\mu} \frac{u_M^{\mu}(\vec{k}_M)\bar{u}_M^{\mu}(\vec{k}_M)}{k_{0M} - E_M}\,.\end{aligned} \tag{3}$$

If we now consider the deuteron wave function $\Psi^*_{M_d\nu\mu}(\vec{p})$ defined by the identification that is valid in the rest frame of the deuteron (which in the region near threshold is very near the ηd rest frame) [12]

$$\frac{M}{E_M} \bar{v}_N^{\nu}(\vec{k}_N) V_{dNN}^{M_d} u_M^{\mu}(\vec{k}_M) \frac{1}{k_{0M} - E_M} \equiv \sqrt{2\omega_d}(2\pi)^{3/2} \Psi^*_{M_d\nu\mu}(\vec{p}), \tag{4}$$

where $\vec{p}$ is the NN relative momentum in the center of mass (c.m.), we obtain from eq. (2)

$$\begin{aligned}A_{M_d}^{\mu_2\mu_3} = \frac{1}{(2\pi)^3} \sum_{\nu\mu} \int \mathrm{d}\vec{k}_N \frac{M}{E_N} \sqrt{2\omega_d} \Psi^*_{M_d\nu\mu}(\vec{p}) \\ \times \bar{u}_M^{\mu}(\vec{k}_M) t_{mN\to\eta N} u_3^{\mu_3}(\vec{k}_3) \\ \times \frac{1}{k_m^2 - m_m^2} \bar{u}_N^{\nu}(\vec{k}_N) V_{mNN} u_2^{\mu_2}(\vec{k}_2).\end{aligned} \tag{5}$$

In eq. (5) we made explicit the momentum dependence of the nucleon spinors.

The deuteron wave function is, on the other hand, calculated from

$$\Psi^*_{M_d\nu\mu}(\vec{p}) = \sum_{\ell=0,2} \sum_{m_\ell, m_S} C^{\ell\ 1\ 1}_{m_\ell m_S M_d} \phi_\ell(p) Y^*_{\ell m_\ell}(\hat{p}) C^{\frac{1}{2}\ \frac{1}{2}\ 1}_{\nu\ \mu\ m_S}\,, \tag{6}$$

where $\phi_0(p)$ and $\phi_2(p)$ are the S- and D-wave components which we obtained from the Paris potential.

For the m meson-nucleon-nucleon vertex we take

$$V_{mNN} = g_m \gamma_5 f_m(k_m^2), \quad m = \pi, \eta, \tag{7}$$

and

$$V_{mNN} = g_m f_m(k_m^2), \quad m = \sigma, \tag{8}$$

where k_m^2 is the meson four-momentum squared and the form factor f_m is chosen to have the monopole form

$$f_m(k_m^2) = \frac{\Lambda^2 - m_m^2}{\Lambda^2 - k_m^2}\,, \tag{9}$$

with $\Lambda = 1200\,\mathrm{MeV}/c$ which is the typical value for meson exchange models [13]. The ηNN coupling constant is not well known since estimates of $g_\eta^2/4\pi$ range from 0.25 to 7 [1]; thus, following [1] we took the reasonable value $g_\eta^2/4\pi = 1$. For the σNN coupling constant we used the value of ref. [13] $g_\sigma^2/4\pi = 8$.

Since the η production near threshold is dominated by the S_{11}-resonance, the m meson-nucleon $\to$ η-nucleon t transition operator is assumed to be generated by a variable-mass isobar model consisting of a single isobar, the S_{11}. As in the framework introduced in ref. [14] for the study of the pion-induced η production reaction, the isobar model for meson-nucleon scattering used here is covariant, and reads

$$t_{mN\to\eta N}(\vec{k}^{\,2},\vec{k}^{\,\prime 2},M_S) = \frac{(2\pi)^2}{M}\sqrt{\omega_m(\vec{p}^{\,2})\omega_\eta(\vec{p}^{\,\prime 2})E(\vec{p}^{\,2})E(\vec{p}^{\,\prime 2})} \times h_m(\vec{p}^{\,2})\frac{\not{k}_M+\not{k}_3+M_S}{2M_S}h_\eta(\vec{p}^{\,\prime 2})\tau(M_S), \quad (10)$$

where $\omega_m(\vec{p}^{\,2}) = \sqrt{m_m^2+\vec{p}^{\,2}}$, $E(\vec{p}^{\,2}) = \sqrt{M^2+\vec{p}^{\,2}}$ are the on-shell energies, respectively, of the m-meson and of the nucleon in the c.m. frame. Also one has

$$M_S = \sqrt{(k_m+k_3)^2} = \sqrt{(k_\eta+k_M)^2}\,. \quad (11)$$

The meson-nucleon-isobar vertices are

$$h_m(\vec{p}^{\,2}) = \sqrt{\frac{2M}{M+E(\vec{p}^{\,2})}}g_m(\vec{p}^{\,2}), \quad m=\pi,\eta \quad (12)$$

and

$$h_m(\vec{p}^{\,2}) = \frac{M}{\sqrt{\vec{p}^{\,2}}}\sqrt{\frac{2M}{M+E(\vec{p}^{\,2})}}g_m(\vec{p}^{\,2})\gamma_5\,, \quad m=\sigma. \quad (13)$$

Here, the three-momentum squared $\vec{p}^{\,2}$ ($\vec{p}^{\,\prime 2}$) is the meson-nucleon relative initial (final) three-momentum in the c.m. frame. In particular, it is given in terms of Lorentz-invariant quantities as

$$\vec{p}^{\,2} = \frac{(M_S^2+M^2-k_m^2)^2}{4M_S^2} - M^2\,. \quad (14)$$

The form factors $g_m(\vec{p}^{\,2})$ and the isobar propagator $\tau(M_S)$ are obtained from a separable potential model describing the ηN-πN-σN two-body subsystem as will be discussed in the next subsection.

In the basis states of the nucleon spinors the matrix element of the transition operator on eq. (10) in the two-body meson-nucleon c.m. system, where $\vec{k}_m+\vec{k}_3 = \vec{k}_\eta + \vec{k}_M = 0$, is given by

$$\bar{u}_M^\mu t_{mN\to\eta N}u_3^{\mu_3} = \delta_{\mu\mu_3}\frac{(2\pi)^2}{M}\sqrt{\omega_m(\vec{p}^{\,2})\omega_\eta(\vec{p}^{\,\prime 2})E(\vec{p}^{\,2})E(\vec{p}^{\,\prime 2})} \times g_m(\vec{p}^{\,2})\tau(M_S)g_\eta(\vec{p}^{\,\prime 2}), \quad (15)$$

and a completely similar expression in the case of the transition $mN \to m'N$ with m or m' any of the mesons.

We consider nucleon 3 with momentum $\vec{q}_N$ in the positive direction of the z-axis and the η-meson three-momentum $\vec{q}_\eta$ in the xz-plane with polar angle θ. Then the amplitude A of eq. (5) satisfies the symmetry property

$$A_{M_d}^{\mu_2\mu_3}(\vec{q}_N,\theta) = -(-1)^{M+\mu_2+\mu_3}A_{M_d}^{\mu_2\mu_3}(-\vec{q}_N,\pi-\theta). \quad (16)$$

In the isospin formalism the neutron and proton are identical particles, so that the initial np state must be antisymmetrized under the exchange of nucleons 2 and 3. However, the system is in a pure total isospin-0 state, which means that the initial np state must be symmetric under the exchange of space and spin variables. Therefore, the correctly antisymmetrized amplitude $B_{M_d}^{\mu_2\mu_3}$ for the $np \to \eta d$ process is

$$B_{M_d}^{\mu_2\mu_3}(q_\eta,q_N,\theta) = \frac{1}{\sqrt{2}}[A_{M_d}^{\mu_2\mu_3}(\vec{q}_N,\theta) + A_{M_d}^{\mu_3\mu_2}(-\vec{q}_N,\theta)] = \frac{1}{\sqrt{2}}[A_{M_d}^{\mu_2\mu_3}(\vec{q}_N,\theta) - (-1)^{M+\mu_2+\mu_3} \times A_{M_d}^{\mu_3\mu_2}(\vec{q}_N,\pi-\theta)]. \quad (17)$$

In the region near threshold the production amplitude (17) is almost independent of θ since the final ηd state is dominated by the orbital angular momentum $L=0$ component. This dominant component can be projected out as

$$B_{M_d}^{\mu_2\mu_3}(q_\eta,q_N) = \frac{1}{2}\int_{-1}^{1}\mathrm{d}\cos\theta\, B_{M_d}^{\mu_2\mu_3}(q_\eta,q_N,\theta). \quad (18)$$

We will apply the initial- and final-state interactions to this dominant amplitude so as to get

$$\bar{B}_{M_d}^{\mu_2\mu_3}(q_\eta,q_N) = \int_0^\infty q_1^2\mathrm{d}q_1\int_0^\infty q_2^2\mathrm{d}q_2 \times\left[\frac{1}{q_1^2}\delta(q_1-q_\eta)+\tau_1(W_0;q_1)T_1(q_1;W_0)\right]B_{M_d}^{\mu_2\mu_3}(q_1,q_2) \times\left[\frac{1}{q_2^2}\delta(q_2-q_N)+\frac{1}{W_0-2\sqrt{m_N^2+q_2^2}+i\epsilon}T_{NN}(q_2;W_0)\right], \quad (19)$$

where W_0 is the total invariant energy, $[(1/q_1^2)\delta(q_1-q_\eta)+\tau_1(W_0;q_1)T_1(q_1;W_0)]$ and $[(1/q_2^2)\delta(q_2-q_N)+T_{NN}(q_2;W_0)/(W_0-2\sqrt{m_N^2+q_2^2}+i\epsilon)]$ are the ηd and NN distorted waves, respectively, which will be discussed in the next two subsections while $B_{M_d}^{\mu_2\mu_3}(q_1,q_2)$ is the off-shell extension of the production amplitude defined by eqs. (18), (17) and (5). Thus, the cross-section of the $np \to \eta d$ process will be obtained as

$$\frac{\mathrm{d}\sigma}{\mathrm{d}\Omega_\eta} = \frac{M^2}{16\pi^2W_0^2}\frac{q_\eta}{q_N}\frac{1}{4}\sum_{\mu_2\mu_3M_d}|\bar{B}_{M_d}^{\mu_2\mu_3}(q_\eta,q_N)|^2\,. \quad (20)$$

2.2 The final-state interaction

In order to generate the ηd distorted wave that appears in eq. (19), we apply to the S-wave ηd elastic channel the realtivistic formalism in momentum space presented in ref. [15]. This formalism generalizes in a straightforward way the nonrelativistic Faddeev equations. It incorporates relativistic kinematics and, importantly, also the boost of the 2-body interactions to the three-body c.m. frame.

Firstly, the main feature of the formalism of [15] consists of a set of relativistic but three-dimensional integral Faddeev-type equations obtained from a field theory in which the three particles are kept on their mass shell in all intermediate states. Accordingly, in what follows the quantity k_i does not refer to the four-momentum of particle i, but to the magnitude of the three-momentum $\vec{k}_i$. Secondly, in order to transform correctly all physical quantities from the two-body to the three-body reference frames, and after considering the energy conservation constraint, one writes the invariant momentum space volume element for the three particles in terms of the two relative Jacobi variables $\vec{p}_i$ and $\vec{q}_i$,

$$\begin{aligned} \mathrm{d}\mathcal{V} &= \frac{\mathrm{d}\vec{k}_1}{2\omega_1(k_1)}\frac{\mathrm{d}\vec{k}_2}{2\omega_2(k_2)}\frac{\mathrm{d}\vec{k}_3}{2\omega_3(k_3)}\delta(\vec{k}_1+\vec{k}_2+\vec{k}_3) \\ &= \frac{\omega(p_i)}{8W_i(p_iq_i)\omega_i(q_i)\omega_j(p_i)\omega_k(p_i)}\mathrm{d}\vec{p}_i\mathrm{d}\vec{q}_i\,. \end{aligned} \tag{21}$$

The variable $\vec{p}_i$ is the relative momentum of the pair jk measured in the c.m. frame of the pair (that is, the frame in which particle j has momentum $\vec{p}_i$ and particle k has momentum $-\vec{p}_i$), and $\vec{q}_i=-\vec{k}_i$ is the relative momentum between the pair jk and the spectator particle i, measured in the c.m. frame of the three particles (in which the pair jk has total momentum $\vec{q}_i$ and particle i has momentum $-\vec{q}_i$). The energy of the jk pair in its c.m. frame is

$$\omega(p_i)=\sqrt{m_j^2+p_i^2}+\sqrt{m_k^2+p_i^2}\,, \tag{22}$$

while in the three-body frame it is

$$W_i(p_i,q_i)=\sqrt{\omega^2(p_i)+q_i^2}\,. \tag{23}$$

Finally, the invariant energy of the three particles is written as

$$W(p_i,q_i)=\omega(q_i)+W_i(p_i,q_i), \tag{24}$$

with

$$\omega_i(q_i)=\sqrt{m_i^2+q_i^2}\,. \tag{25}$$

Equations (21)–(25) determine the transformation of the matrix elements of the two-body potential V, given in the two-body c.m. frame by $V(\vec{p}_i,\vec{p}_i')$, to the three-body c.m. reference frame, as found in [15]:

$$\begin{aligned} &\langle\vec{p}_i\vec{q}_i|V|\vec{p}_i'\vec{q}_i'\rangle = \\ &\left[\frac{W_i(p_iq_i)\omega_j(p_i)\omega_k(p_i)W_i(p_i'q_i)\omega_j(p_i')\omega_k(p_i')}{\omega(p_i)\omega(p_i')}\right]^{1/2} \\ &\times\delta(\vec{q}_i-\vec{q}_i')8\omega_i(q_i)V(\vec{p}_i,\vec{p}_i'), \end{aligned} \tag{26}$$

which in turn defines the boosted matrix element of the two-body t-matrix. These are given by

$$\begin{aligned} &\langle\vec{p}_i\vec{q}_i|t(W_0)|\vec{p}_i'\vec{q}_i'\rangle = \\ &\left[\frac{W_i(p_iq_i)\omega_j(p_i)\omega_k(p_i)W_i(p_i'q_i)\omega_j(p_i')\omega_k(p_i')}{\omega(p_i)\omega(p_i')}\right]^{1/2} \\ &\times\delta(\vec{q}_i-\vec{q}_i')8\omega_i(q_i)t(\vec{p}_i,\vec{p}_i';W_0,q_i), \end{aligned} \tag{27}$$

where $t(\vec{p}_i,\vec{p}_i';W_0,q_i)$ satisfies the Lippmann-Schwinger equation with a propagator corresponding to relativistic kinematics defined by eq. (24):

$$\begin{aligned} t(\vec{p}_i,\vec{p}_i';W_0,q_i) = V(\vec{p}_i,\vec{p}_i') + \int \mathrm{d}\vec{p}_i''V(\vec{p}_i,\vec{p}_i'') \\ \times\frac{1}{W_0-W(p_i''q_i)+i\epsilon}t(\vec{p}_i'',\vec{p}_i';W_0,q_i). \end{aligned} \tag{28}$$

The variable W_0, as mentioned in the previous subsection, is the invariant energy of the three-body system. For only S-wave two-body interactions eq. (28) becomes

$$\begin{aligned} t(p_i,p_i';W_0,q_i) = V(p_i,p_i') + \int_0^\infty p_i''^2\mathrm{d}p_i''V(p_i,p_i'') \\ \times\frac{1}{W_0-W(p_i''q_i)+i\epsilon}t(p_i'',p_i';W_0,q_i). \end{aligned} \tag{29}$$

In the particular case of the coupled ηN-πN-σN subsystem these three different meson-nucleon channels are connected among each other through the S_{11} partial wave. For each transition, we use rank-one separable potentials of the form

$$V_{mm'}(p_i,p_i')=-g_m(p_i)g_{m'}(p_i');\quad (m,m'=\eta,\pi,\sigma). \tag{30}$$

The solution of eq. (29) is

$$t_{mm'}(p_i,p_i';W_0,q_i)=g_m(p_i)\tau_2(W_0;q_i)g_{m'}(p_i'), \tag{31}$$

with

$$\tau_2^{-1}(W_0;q_i)=-1-\sum_{m=\eta,\pi,\sigma}\int_0^\infty p_i^2\mathrm{d}p_i\frac{g_m^2(p_i)}{W_0-W(p_iq_i)+i\epsilon}\,. \tag{32}$$

We will now check the consistency between the results for the boosted two-body t-matrix derived in this section, and the result for the covariant two-body matrix elements introduced in the previous subsection. If we substitute eq. (32) into eq. (27) and take $q_i=0$ we obtain

$$\begin{aligned} \langle\vec{p}_i\vec{0}|t(W_0)|\vec{p}_i'\vec{q}_i'\rangle = [\omega_j(p_i)\omega_k(p_i)\omega_j(p_i')\omega_k(p_i')]^{1/2} \\ \times\delta(\vec{0}-\vec{q}_i')8m_i\,g_m(p_i)\tau_2(W_0)g_{m'}(p_i'). \end{aligned} \tag{33}$$

From eqs. (33) and (15) we conclude that the t-matrix element dynamically generated from the separable potential model of eq. (30) and the relativistic scattering equation, coincides with the covariant matrix element of eq. (15) obtained in the basis of the nucleon spinors. The different multiplicative factors ($8m_i$ *vs.* $(2\pi)^2/M$) originate from

the normalization convention for two-body momentum basis states used in Faddeev-type formalisms.

We test two different types of vertex functions $g_m(p_i)$ in the fits of the meson-nucleon scattering data analysed, in order to assess the extent of the model dependence of the results. The two types of functions with different falling-off behavior for large values of the momenta are models labeled as type I, with a dipole form

$$g_m(p_i) = \sqrt{\lambda_m}\frac{A_m + p_i^2}{(\alpha_m^2 + p_i^2)^2}\,; \quad (m = \eta, \pi), \tag{34}$$

$$g_m(p_i) = \sqrt{\lambda_m}\frac{p_i}{(\alpha_m^2 + p_i^2)^2}\,; \quad (m = \sigma) \tag{35}$$

and models labeled as type II, which have a tail of Gaussian form

$$g_m(p_i) = \sqrt{\lambda_m}(A_m + p_i^2)e^{-2p_i^2/\alpha_m^2}\,; \quad (m = \eta, \pi), \tag{36}$$

$$g_m(p_i) = \sqrt{\lambda_m}p_i e^{-2p_i^2/\alpha_m^2}\,; \quad (m = \sigma). \tag{37}$$

The parameters of these models were obtained by fitting the $\eta N \to \eta N$ amplitude of the amplitude analyses of refs. [7–10] (as well as the interpolated models that will be described in the next section) and the $\pi N \to \eta N$ cross-section for c.m. energies below 100 MeV (see for example ref. [3]).

In the case of the $^3S_1$ NN interaction we used the PEST separable potential [16]

$$V_{NN}(p_i, p_i') = -g_N(p_i)g_N(p_i'), \tag{38}$$

with

$$g_N(p_i) = 0.88772\sum_{n=1}^{6}\frac{c_n}{\beta_n^2 + p_i^2}\,, \tag{39}$$

and the parameters c_n and β_n given in ref. [16]. The solution of eq. (29) for the potential (38) is

$$t_{NN}(p_i, p_i'; W_0, q_i) = g_N(p_i)\tau_1(W_0; q_i)g_N(p_i'), \tag{40}$$

with

$$\tau_1^{-1}(W_0; q_i) = -1 - \int_0^\infty p_i^2 \mathrm{d}p_i \frac{g_N^2(p_i)}{W_0 - W(p_i q_i) + i\epsilon}\,. \tag{41}$$

The potential (38) has a bound-state solution at the energy of the deuteron and its wave function at low momentum coincides with the deuteron wave function of the Paris potential.

Using these separable interactions the integral equations for ηd elastic scattering are

$$T_1(q_1; W_0) = 2\int_0^\infty {q_2}^2 \mathrm{d}q_2 K_{12}(q_1, q_2; W_0) \times\tau_2(W_0; q_2)T_2(q_2; W_0), \tag{42}$$

$$T_2(q_2; W_0) = 2K_{21}(q_2, q_{10}; W_0) + \int_0^\infty {q_2'}^2 \mathrm{d}q_2' \times K_{23}(q_2, q_2'; W_0)\tau_2(W_0; q_2')T_2(q_2'; W_0) + \int_0^\infty q_1^2 \mathrm{d}q_1 K_{21}(q_2, q_1; W_0)\tau_1(W_0; q_1)T_1(q_1; W_0). \tag{43}$$

In these equations $T_1(q_1; W_0)$ is the ηd elastic scattering amplitude (which appears in the ηd distorted wave in eq. (19), while the function $T_2(q_2; W_0)$ is the transition amplitude from the ηd state to a state with a nucleon and a S_{11} isobar. (The transition matrix index labels the spectator particle —1 for the η and 2,3 for the two nucleons.) These half-off-shell scattering matrices depend on the invariant mass of the ηd system given by $W_0 = \sqrt{m_\eta^2 + q_{10}^2} + \sqrt{m_d^2 + q_{10}^2}$, where q_{10} is the on-shell momentum. The variables q_1 and q_2 are, respectively, the η-d and the S_{11}-nucleon relative momenta in the three-body center of mass. The kernels K_{21} and K_{23} stand, respectively, for the exchange of a nucleon and of a (π-, η- and σ-) meson, the subscripts refer to the spectator particles before and after the exchange. They are given by [15]

$$K_{12}(q_1, q_2; W_0) = K_{21}(q_2, q_1; W_0) = \frac{1}{2}\int_{-1}^{1}\frac{\mathrm{d}\cos\theta}{\sqrt{m_3^2 + q_1^2 + q_2^2 + 2q_1q_2\cos\theta}} \times\left[\frac{W_1(p_1q_1)\omega_2(p_1)\omega_3(p_1)W_2(p_2q_2)\omega_3(p_2)\omega_1(p_2)}{\omega(p_1)\omega(p_2)\omega_1(q_1)\omega_2(q_2)}\right]^{1/2} \times\frac{g_N(p_1)g_\eta(p_2)}{W_0 - W(p_2q_2) + i\epsilon}\,, \tag{44}$$

and

$$K_{23}(q_2, q_3; W_0) = K_{23}^{\eta}(q_2, q_3; W_0) - K_{23}^{\pi}(q_2, q_3; W_0) + K_{23}^{\sigma}(q_2, q_3; W_0), \tag{45}$$

where the superscripts η, π, and σ in the r.h.s of eq. (45) indicate which meson is particle 1, while

$$K_{23}^{m}(q_2, q_3; W_0) = \frac{1}{2}\int_{-1}^{1}\frac{\mathrm{d}\cos\theta}{\sqrt{m_1^2 + q_2^2 + q_3^2 + 2q_2q_3\cos\theta}} \times\left[\frac{W_2(p_2q_2)\omega_3(p_2)\omega_1(p_2)W_3(p_3q_3)\omega_1(p_3)\omega_2(p_3)}{\omega(p_2)\omega(p_3)\omega_2(q_2)\omega_3(q_3)}\right]^{1/2} \times\frac{g_m(p_2)g_m(p_3)}{W_0 - W(p_3q_3) + i\epsilon}\left[(1 - \delta_{m\sigma}) + \delta_{m\sigma}\frac{\hat{p}_2\cdot\hat{p}_3}{3}\right]; \quad m = \eta, \pi, \sigma. \tag{46}$$

In eqs. (44) and (46) one can obtain p_i, p_j and $\hat{p}_i\cdot\hat{p}_j$ using

$$\vec{p}_i = -\vec{q}_j - \alpha_{ij}(q_iq_j\cos\theta)\vec{q}_i\,, \tag{47}$$

$$\vec{p}_j = \vec{q}_i + \alpha_{ji}(q_iq_j\cos\theta)\vec{q}_j\,, \tag{48}$$

with

$$\alpha_{ij}(q_iq_j\cos\theta) = \frac{W_i^2 - q_i^2 + m_j^2 - m_k^2 + 2\omega_j(q_j)\sqrt{W_i^2 - q_i^2}}{2\sqrt{W_i^2 - q_i^2}\left[W_i + \sqrt{W_i^2 - q_i^2}\right]}\,, \tag{49}$$

$$\alpha_{ji}(q_iq_j\cos\theta) = \frac{W_j^2 - q_j^2 + m_i^2 - m_k^2 + 2\omega_i(q_i)\sqrt{W_j^2 - q_j^2}}{2\sqrt{W_j^2 - q_j^2}\left[W_j + \sqrt{W_j^2 - q_j^2}\right]}\,, \tag{50}$$

and

$$W_i = \sqrt{m_j^2 + q_j^2} + \sqrt{m_k^2 + q_i^2 + q_j^2 + 2q_i q_j \cos\theta}\,, \quad (51)$$

$$W_j = \sqrt{m_i^2 + q_i^2} + \sqrt{m_k^2 + q_i^2 + q_j^2 + 2q_i q_j \cos\theta}\,. \quad (52)$$

Notice that in eq. (45) the contribution of the η comes with a plus sign while the contribution of the π comes with a minus sign. These signs arise from the reduction of the Faddeev equations when one has two identical fermions [17,18]. Since we are assuming that the meson is particle 1 so that 2 and 3 are the two fermions and for the π and η all orbital angular momenta are equal to zero, then following the reduction procedure of refs. [17, 18] leads to that result. In the case of the σ the orbital angular momentum of the pair and the total orbital angular momentum are $\ell = L = 1$ so that the derivation of the kernel is slightly more complicated as shown, for example, in ref. [17] with the result that it appears in eq. (46) for $m = \sigma$.

Since the energies that we consider in this work are in the continuum, we deal with the three-body singularities by using the method of contour rotation [19].

2.3 The initial NN interaction

In the case of the np initial-state interaction we used the optical potential

$$V_{NN}(q_2, q_2') = V_{PARIS}(q_2, q_2') - i\gamma \frac{q_2 q_2'}{(\alpha^2 + q_2^2)(\alpha^2 + q_2'^2)}\,, \quad (53)$$

where the parameters $\gamma = 0.8$ and $\alpha = 0.3\,\mathrm{fm}^{-1}$ were obtained by reproducing the $np\ ^1P_1$ amplitude of Arndt *et al.* [20] at the η threshold. The NN half-shell t-matrix $T_{NN}(q_2; W_0)$ is then obtained by solving the relativistic Lippmann-Schwinger equation

$$T_{NN}(q_2; W_0) = V_{NN}(q_2, q_{20}) + \int_0^\infty q_2'^2 \mathrm{d}q_2' V_{NN}(q_2, q_2') \times \frac{1}{W_0 - 2\sqrt{M^2 + q_2'^2} + i\epsilon} T_{NN}(q_2'; W_0), \quad (54)$$

where $q_{20} = \sqrt{W_0^2/4 - M^2}$ is the on-shell momentum.

3 New aspects of the calculation

Given the dominant role of the S_{11} ηN amplitude as a mechanism for the $np \to \eta d$ process, and at the same time the sensitivity of the results of the cross-section as a function of the energy to details to that amplitude, it becomes necessary to develop a description of it, as much realistic as possible. Thus, in the region near threshold, the ηN amplitude must contain contributions from the ηN, πN, and $\pi\pi N$ coupled channels, all three observed experimentally to be important. In the previous section we constructed two sets of models of the ηN amplitude (models of type I and type II corresponding, respectively, to dipole and Gaussian form factors) where the ηN, πN, and σN channels were included and where a stable σ with a mass m_σ effectively represents the $\pi\pi$ channel. In order to assess the effects of this approximate treatment of the $\pi\pi$ channel, we have now replaced, in the 3- and 2-body propagators entering into the dynamical equations of the previous section, the constant mass of the σ-meson by the energy-dependent function

$$m_\sigma \to \sqrt{s_0} - \frac{i}{2}\Gamma(\sqrt{s_\sigma}), \quad (55)$$

where $\sqrt{s_0} = 850\,\mathrm{MeV}$ is the $\pi\pi$ c.m. energy at which the $I = J = 0$ $\pi\pi$ phase shift passes through 90° [21] and

$$\Gamma(\sqrt{s_\sigma}) = 0; \quad \sqrt{s_\sigma} \le 2m_\pi\,, \quad (56)$$

$$\Gamma(\sqrt{s_\sigma}) = 2(\sqrt{s_0} - \sqrt{s_\sigma}) \frac{k}{k\,\mathrm{cotg}\,\delta}; \quad \sqrt{s_\sigma} > 2m_\pi\,. \quad (57)$$

Furthermore, using the $I = J = 0$ $\pi\pi$ phase shift of ref. [21] we obtained (k given in fm^{-1})

$$k\,\mathrm{cotg}\,\delta = 2.224 - 1.038k^2 + 0.181k^4\,. \quad (58)$$

k and s_σ are the c.m. momentum and invariant-mass squared of the $\pi\pi$ system, respectively, given by

$$k = \frac{1}{2}\sqrt{s_\sigma - 4m_\pi^2}\,, \quad (59)$$

$$s_\sigma = (\omega_0 - \sqrt{M^2 + p^2})^2 - p^2\,, \quad (60)$$

$$\omega_0^2 = [W_0 - \sqrt{M^2 + q^2}]^2 - q^2\,, \quad (61)$$

where W_0 is the total energy, p is the relative momentum of the meson-nucleon subsystem and q is the relative momentum of the meson-nucleon subsystem with respect to the other nucleon.

In order to generate models of the ηN-ηN amplitude with $\mathrm{Re}(a_{\eta N})$ in between those of models 0–6 [7–10], we considered the dependence on the continuous variable $x = \mathrm{Re}(a_{\eta N})$, of all of the three complex low-energy parameters for the two-body scattering amplitude:

$$a = a_{\eta N}(x) = \sum_{n=0}^{3} b_n x^n\,, \quad (62)$$

$$r = r_{\eta N}(x) = \sum_{n=0}^{3} c_n x^n\,, \quad (63)$$

$$s = s_{\eta N}(x) = \sum_{n=0}^{3} d_n x^n\,. \quad (64)$$

To be able to describe the $np \to \eta d$ reaction, and as in refs. [1] and [3], our calculations here include, not only the reaction mechanisms originated by π, η and σ exchanges, $M_{\pi+\eta+\sigma}$, but also a short-range exchange mechanism involving the virtual exchange of a pseudoscalar meson η' with a mass 957 MeV and vertices $V_{\eta' NN}$ given by eq. (7) and $V_{\eta' NS_{11}}$ given by eq. (8). It is worth mentioning that

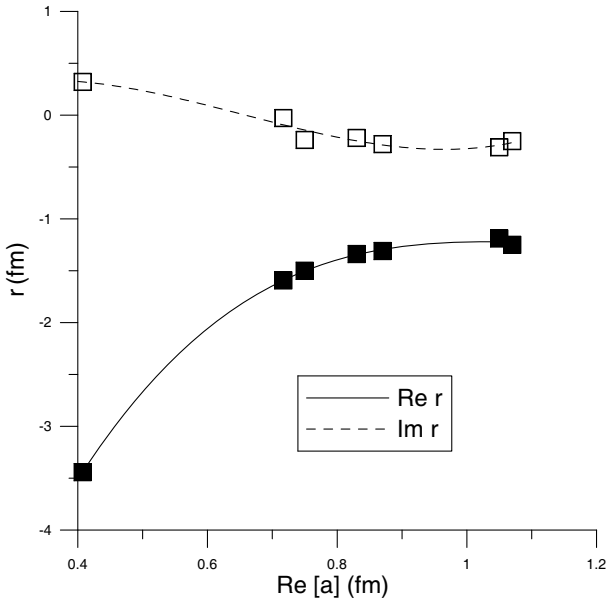

Fig. 1. ηN effective range r for the seven models 0–6 and as given by the expansion (63).

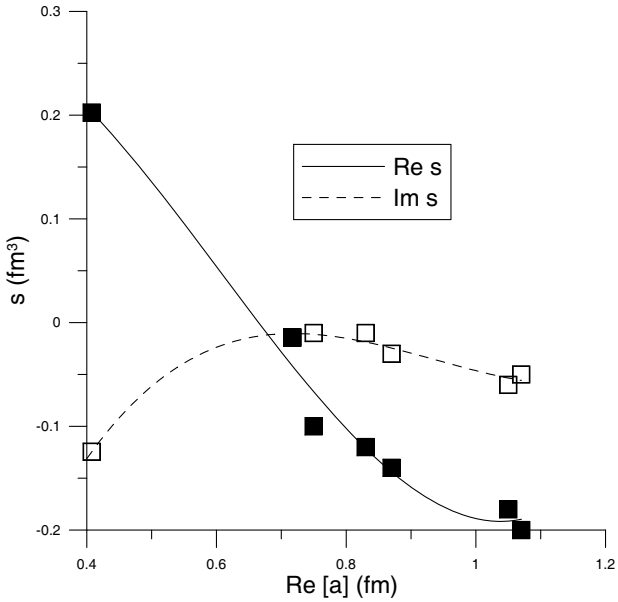

Fig. 2. ηN shape parameter s for the seven models 0–6 and as given by the expansion (64).

we checked in ref. [3] that the exchange of a vector or a scalar meson instead of a pseudoscalar one would lead to similar results. We can combine the two contributions, obtaining the cross-section from

$$\sigma = |M_{\pi+\eta+\sigma} + g_{\eta' NN} g_{\eta' NS_{11}} A_{\eta'}|^2 \,, \qquad (65)$$

where we separated in the second term the product of the couplings involved, $g_{\eta' NN} g_{\eta' NS_{11}}$, from the rest of the amplitude, $A_{\eta'}$, in order to exhibit the freedom to explore both the positive and a negative coupling cases, which we investigated, as discussed in the next section.

Table 2. Coefficients of the expansion of the effective-range parameters.

Parameter	$n=0$	$n=1$	$n=2$	$n=3$
$\mathrm{Re}\, b_n$	0	1	0	0
$\mathrm{Im}\, b_n$	0.330	−0.410	0.693	−0.344
$\mathrm{Re}\, c_n$	−10.007	23.708	−21.200	6.275
$\mathrm{Im}\, c_n$	−0.526	5.672	−11.125	5.655
$\mathrm{Re}\, d_n$	0.223	0.807	−2.709	1.489
$\mathrm{Im}\, d_n$	−0.878	3.047	−3.443	1.227

4 Results and conclusions

We show in figs. 1 and 2 the effective-range parameter r and the shape parameter s obtained from the analyses of models 0–6 together with the minimum-square fit of them that we obtained through eqs. (62)–(64). The parameters b_n, c_n, and d_n are given in table 2. What figs. 1 and 2 show is that the effective-range parameters of the seven models are strongly correlated among themeselves which, of course, is a reflection of the fact that they were fitted to the same set of data. We note from table 1 that all models are consistent with a small value of the imaginary part of the scattering length, which does not depend much on the particular model. In contrast, the real part of the effective-range r depends critically on the ηN model, as seen in fig. 1, although its imaginary part lies close to zero. The shape parameter s, shown in fig. 2, is roughly one order of magnitude smaller than the other two parameters so that its effect will be negligible at energies near threshold. This fit allowed us to obtain models for ηN-ηN scattering by dialing the values of $\mathrm{Re}(a_{\eta N})$. It is noticeable the rapid variation of $\mathrm{Re}(r)$ in the region of small $\mathrm{Re}(a_{\eta N})$, which is likely to be related to the sensitivity of the $np \to \eta d$ cross-section to the ηN models observed in refs. [1] and [3].

In fig. 3 we include the results for the cross-section of the $np \to \eta d$ reaction for models 0 [10], 1 [7], and 6 [9] plus three models interpolating between the data analyses 0 [10] and 1 [7]. More precisely, the six curves correspond to values of $x = \mathrm{Re}(a_{\eta N}) = 0.41$ (model 0), 0.45, 0.50, 0.55, 0.72 (model 1), and 1.07 (model 6) fm.

In this figure all results correspond to the treatment of the $\pi\pi$ channel by means of a σ-meson with a width. What is the role of the σ width in the $np \to \eta d$ calculation? To answer that we show in fig. 4 the same as in fig. 3, but for the case where the σ mass is constant and given by $2m_\pi$. Although not essential, the σ width implies some repulsion in the $\pi\pi$ channels, and henceforth indirectly through unitarity it enhances the ηN attraction effect. This is why with inclusion of the σ width the favored model is the Jülich model, model 0 (with $x = 0.41$), while without the σ width the reaction involving a 3-body final state requires the stronger ηN interaction strength of the model with $x = 0.45$.

In fig. 5 we show, for the case of the σ width being included, the results for the 4 models that satisfactorily

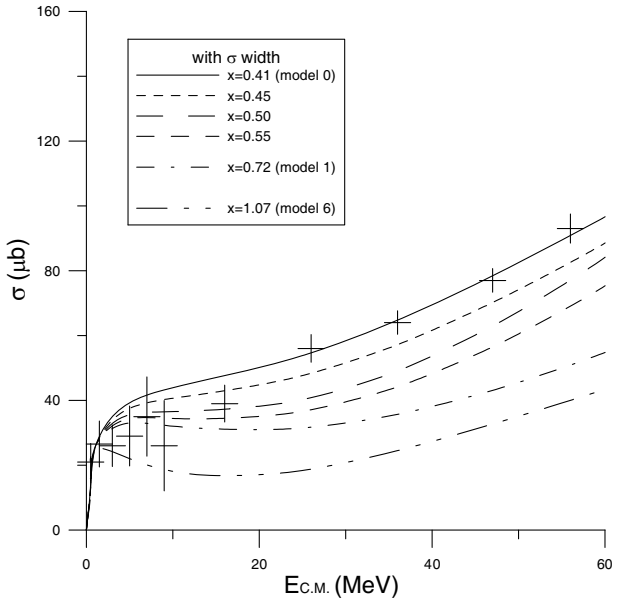

Fig. 3. Cross-section of the $np \to \eta d$ process with σ width included using a dipole form factor for the ηN interaction and a positive heavy-meson coupling strength. Results are shown for the models 0, 1, and 6 plus the models with $x = 0.45$, 0.50, and 0.55.

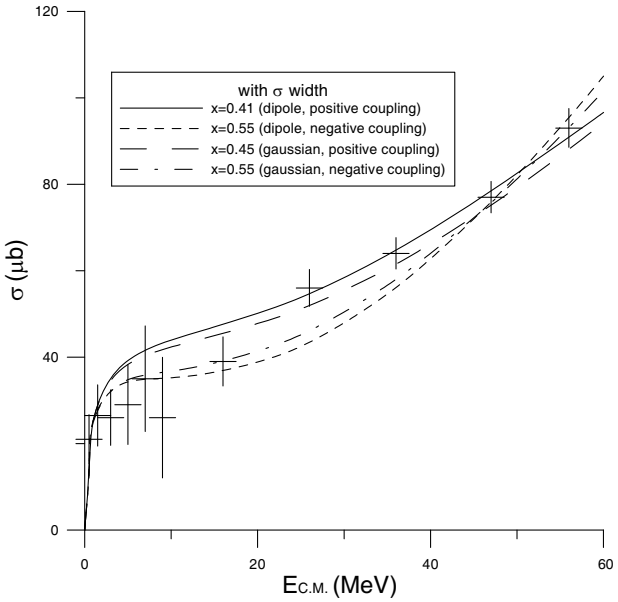

Fig. 5. Results for the cross-section of the $np \to \eta d$ reaction for the 4 cases that best describe the data with σ width included. The curves correspond, as indicated, to dipole or Gaussian form factors for the ηN interaction, and positive or negative heavy-meson coupling strength.

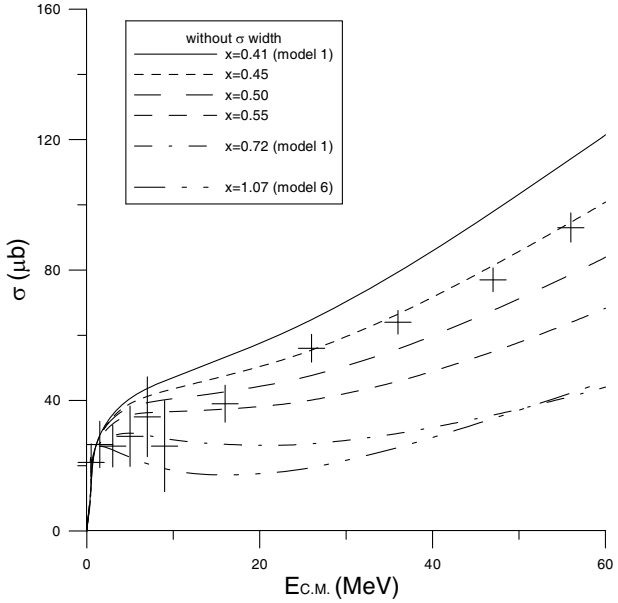

Fig. 4. The same as fig. 4 for the case without σ width.

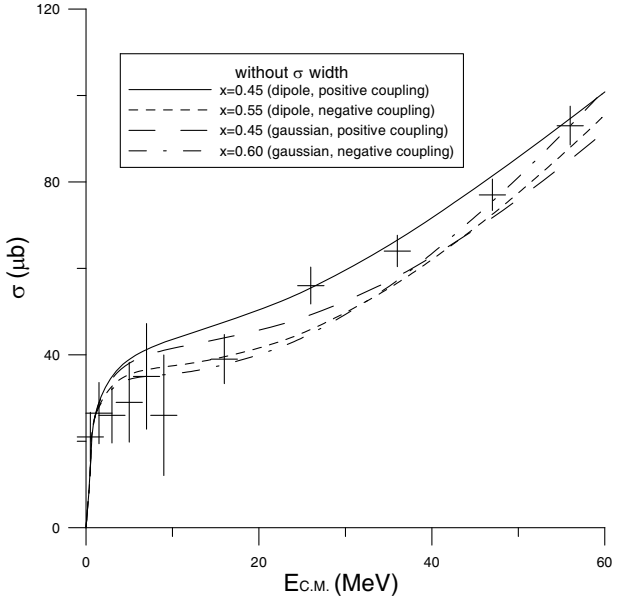

Fig. 6. The same as fig. 5 but for the corresponding cases without the σ width included.

describe the $np \to \eta d$ reaction. The figure compares the results obtained with a dipole form for the ηN separable interaction to the ones with a Gaussian form for that interaction. The figure includes also the results for the two possible signs for the short-range coupling, as discussed in the previous section. A negative sign increases slightly the ηN scattering length needed for the description of the $np \to \eta d$ reaction, to compensate the negative interference between the $\pi+\eta+\sigma$ and the shorter-range exchanges. Notice that the effect of the sign of the short-range coupling is more decisive very near threshold, since this is where the strength of the ηN scattering is needed (high momentum transfer region). However, this is not visible in the curves because they are obtained by fixing the strength of the short-range interaction to the data near threshold. This procedure makes the curves differ in the high-energy region. In fig. 6 we show the same as fig. 5, but when a constant mass is taken for the σ effective meson. The results of figs. 5 and 6 indicate, as seen already from figs. 3 and 4,

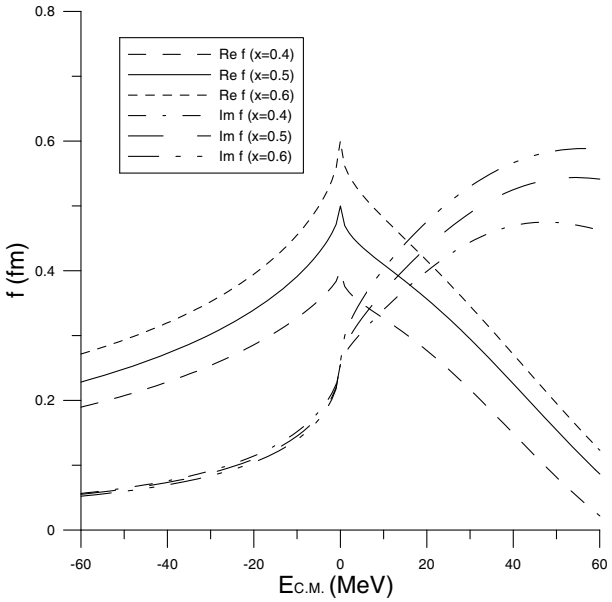

Fig. 7. ηN-ηN scattering amplitude f as a function of energy for the allowed values $x = 0.4$, 0.5, and 0.6.

that independently of the form factor having a dipole or a Gaussian form, the repulsion in the π-π channels caused by the σ width enhances the ηN scattering effect, allowing a smaller scattering length value. From both figures, we emphasize also that the off-shell differences in the models (dipole form *vs.* Gaussian form factor models), which can be read from comparing the solid to the short-dashed and the dashed to the dash-dotted lines, are smaller than the experimental error bar uncertainties.

Finally, we note that our calculation is strictly valid only in the region below 60 MeV away from threshold, given that we consider only s-wave η production, which is dominant in this region. In summary, the $np \to \eta d$ cross-section is well described up to about 60 MeV, and it helps constraining the ηN interaction. It indicates that the real part of the ηN scattering length lies between $0.4 < x < 0.6$ fm. Thus, we conclude that $\mathrm{Re}(a_{\eta N}) = 0.5 \pm 0.1$ fm. As an application of this result and the expansions (62)–(64) we show in fig. 7 the scattering amplitude f defined by

$$f^{-1} = \frac{1}{a} + \frac{1}{2} r p^2 + s p^4 - ip, \tag{66}$$

using for x the allowed values 0.4, 0.5, and 0.6 for energies between -60 and 60 MeV, which is the range of validity of our analysis.

This work was supported in part by COFAA-IPN (Mexico) and by Fundação para a Ciência e a Tecnologia, under contract POCTI/FNU/50358/2002.

References

1. H. Garcilazo, M.T. Peña, Phys. Rev. C **72**, 014003 (2005).
2. H. Garcilazo, M.T. Peña, Phys. Rev. C **61**, 064010 (2000); **63**, 021001 (2001).
3. H. Garcilazo, M.T. Peña, Phys. Rev. C **66**, 034606 (2002).
4. H. Calén *et al.*, Phys. Rev. Lett. **79**, 2642 (1997); H. Calén *et al.*, Phys. Rev. Lett. **80**, 2069 (1998).
5. K.M. Watson, Phys. Rev. **88**, 1163 (1952).
6. A. Sibirtsev, S. Schneider, Ch. Elster, J. Haidenbauer, S. Krewald, J. Speth, Phys. Rev. C **65**, 044007 (2002) (Old model 0).
7. M. Batinić, I. Šlaus, A. Švarc, B.M.K. Nefkens, Phys. Rev. C **51**, 2310 (1995); M. Batinić, I. Dadić, I. Šlaus, A. Švarc, B.M.K. Nefkens, T.-S.H. Lee, Phys. Scr. **58**, 15 (1998) (Model 1).
8. A.M. Green, S. Wycech, Phys. Rev. C **55**, R2167 (1997) (Model 2).
9. A.M. Green, S. Wycech, Phys. Rev. C **60**, 035208 (1999) (Models 3–6).
10. A.M. Gasparian, J. Haidenbauer, C. Hanhart, Phys. Rev. C **68**, 045207 (2003) (New model 0).
11. W. Grein, A. König, P. Kroll, M.P. Locher, A. Švarc, Ann. Phys. **153**, 301 (1984).
12. W.W. Buck, F. Gross, Phys. Rev. D **20**, 2361 (1979).
13. R. Machleidt, K. Holinde, C. Elster, Phys. Rep. **149**, 1 (1987).
14. H. Garcilazo, M.T. Peña, Phys. Rev. C **59**, 2389 (1999).
15. H. Garcilazo, Phys. Rev. C **67**, 055203 (2003).
16. H. Zankel, W. Plessas, J. Haidenbauer, Phys. Rev. C **28**, 538 (1983).
17. H. Garcilazo, T. Mizutani, *πNN Systems* (World Scientific, Singapore, 1990).
18. I.R. Afnan, A.W. Thomas, Phys. Rev. C **10**, 109 (1974).
19. J.H. Hetherington, L.H. Schick, Phys. Rev. **137**, B935 (1965).
20. R.A. Arndt, I.I. Strakovsky, R.L. Workman, Phys. Rev. C **62**, 034005 (2000).
21. C.D. Frogatt, J.L. Peterson, Nucl. Phys. B **129**, 89 (1977).